Fourier ptychography algorithm based on scaled Fourier transform

Mojde Hasanzade,[1] Nazabat Hussain,[1] Dag W. Breiby,[1,2] and Muhammad N. Akram[1]

[1]*Department of Microsystems, University of South-Eastern Norway, Tonsberg, Norway*

[2]*PoreLab, Department of Physics, Norwegian University of Science and Technology, Trondheim, Norway*

This letter discusses an alternative Fourier ptychography algorithm based on the scaled fast Fourier transform propagation. The advantage of this scheme is that it enables a zoom-in capability of the object spectrum and complex pupil within the synthetic numerical aperture without increasing the overall matrix size. Thus, the high-resolution complex object and complex pupil are recovered utilising a larger fraction of the elements in their respective representation matrices. Experimental results are presented showing the performance of this scheme against the tradition fast-Fourier-transform-based approach.

Introduction: Fourier ptychography microscopy (FPM) is a well-known coherent imaging technique for achieving resolution beyond the diffraction limit while simultaneously retrieving the unknown phase information of a complex object [1–5]. In the FPM scheme, the object is illuminated by a coherent or partially coherent light source, and a number of low-resolution intensity images are captured by a digital camera. The highest spatial frequency in the captured images is limited by the coherent transfer function (CTF) of the optics. The digital camera spatially samples the image, and its Nyquist sampling frequency defines the maximum un-aliased spatial frequency that can be faithfully represented in the captured image [1, 6]. By illuminating the object at different angles from different LEDs, the extended object spectrum gets shifted in the Fourier plane, and thus, different sub-parts of this spectrum get passed through the CTF of the lens and ultimately reach the camera plane. The camera records the squared absolute value of the electric field, while the phase information of the electric field is lost. Eventually, this field propagation process is simulated in the software, and by exploiting different sub-spectra together along with iteratively propagating the electric field back and forth between the camera plane and the Fourier plane while using the recorded information of the absolute electric field, the complex extended Fourier spectrum is recovered, which is equivalent to recovering the complex object information with much higher final spatial resolution. In the FPM scheme, the synthesised numerical aperture (NA) is equal to the sum of optical NA and illumination NA. Many improvements have been made to the basic FPM algorithm, such as high NA implementation [7], adaptive system correction [8], unknown complex pupil function or aberration recovery [5, 9], thick sample recovery [10], different denoising methods [11] and Fresnel-integral-based wave propagation [12, 13], to name a few.

In all these schemes, the fast Fourier transform (FFT) algorithm for discrete Fourier transform (DFT) calculation is used to calculate the spectrum of the object. The FFT algorithm defines a fixed relation between the spatial sampling period δx and the spectral sampling period $\delta f = 1/(N\delta x)$, where $N \times N$ is the matrix size to represent the discretised complex high-resolution object or its spectrum. With the FFT algorithm, the spectrum matrix at the Fourier plane extends far beyond the optical synthetic cut-off frequency. As a result, only a small portion of the calculated spectrum matrix up to the synthetic cut-off frequency is utilised in the FPM recovery process, wasting a big part of the spectrum matrix. This letter proposes to use the scaled Fourier transform algorithm (sometimes also called the fractional Fourier transform) [14–16] to compute the spectrum of the object and implement the forward–backward field propagation steps in the FPM scheme. The scaled FFT provides the capability of zooming-in into the object spectrum. Thus, most of the calculated spectrum matrix contains field information that is useful in the FPM recovery, and the object spectrum is sampled with more elements without increasing the overall matrix size. In addition, the optical CTF is also sampled with more elements showing finer details.

Scaled fourier transform algorithm: Based on [14–16], the one-dimensional scaled Fourier transform of $h(j)$ can be written as

$$\begin{aligned} H(k) &= \sum_j h(j)\exp(-i2\pi sjk) \\ &= \sum_j h(j)\exp(-i\pi s[j^2+k^2-(k-j)^2]) \\ &= \exp(-i\pi sk^2)\sum_j h(j)\exp(-i\pi sj^2)\exp(i\pi s(k-j)^2) \\ &= \exp(-i\pi sk^2)\sum_j \chi(j)\zeta(k-j) \\ &= \exp(-i\pi sk^2)[\chi(j)\otimes\zeta(k)] \\ &= \exp(-i\pi sk^2)\mathrm{FFT}^{-1}[\mathrm{FFT}\{\chi(j)\}\mathrm{FFT}\{\zeta(k)\}] \end{aligned} \quad (1)$$

where $k = 0, 1, \ldots, N-1$ is the frequency index, $j = 0, 1, \ldots, N-1$ is the spatial index, N is the array size, s is the Fourier transform scaling parameter, $\chi(j) = h(j)\exp(-i\pi sj^2)$, $\zeta(k-j) = \exp(i\pi s(k-j)^2)$ and $\otimes$ is the convolution operator. The convolution can be implemented in the frequency domain by first zero padding the input array to make it of size $2N$, taking its Fourier transform, multiplying it with the Fourier transform of $\zeta(k)$ (which is also padded to the size $2N$), then taking the inverse Fourier transform of the product and selecting only the valid part of size N from the output array of total size $2N$ [14, 16]. To save one FFT operation, the analytical Fourier transform of $\zeta(k)$ can also be sampled and used in the calculations. Choosing the scaling parameter $s = 1/N$ results in the traditional DFT with spatial sampling period δx, spectral sampling period $\delta f = 1/(N\delta x)$ and maximum frequency in the calculated spectrum $f_{\max} = 1/(2\delta x)$. Alternatively, by choosing $s = s_1/N$, where $s_1 < 1.0$, the spectral sampling period becomes $\delta f = s_1/(N\delta x)$ and the maximum frequency in the calculated spectrum becomes $f_{\max} = s_1/(2\delta x)$. We explain here with an example in the FPM context. For a reconstructed high-resolution sample with spatial resolution $\delta x = 148.8$ nm and matrix size 2048×2048, circular synthetic numerical aperture $\mathrm{NA}_{\mathrm{synth}} = 0.34$, the maximum spatial frequency in the usual DFT will be $f_{\max} = 3.3583 \times 10^6$ m^{-1} and the maximum spatial frequency reached by the synthetic NA is $f_{\max,\mathrm{synth}} = \mathrm{NA}_{\mathrm{synth}} \times k_0/(2\pi) = 6.548 \times 10^5$ m^{-1}. Thus, all the calculated frequencies in the object spectrum matrix outside the circle with radius $f_{\max,\mathrm{synth}}$ are not utilised in the FPM reconstruction, wasting approximately 97% portion of the object spectrum matrix. If we choose the scaling parameter $s_1 = 0.25$ in the scaled FFT, the maximum spatial frequency in the calculated spectrum will be $f_{\max} = 8.395 \times 10^5$ m^{-1}, which results in 47.8% portion of the calculated spectrum matrix actually being utilised in the FPM reconstruction, and thus, the object spectrum (and the unknown complex pupil, which is a scaled version of the lens CTF [6]) will be sampled with more elements.

Pseudo-MATLAB code: Based on (1), we have programmed a function ScaledFFT in MATLAB. The scaling parameter s is positive for forward and negative for the inverse scaled FFT. The scaled-Fourier-transform-based ptychography algorithm is implemented, which is a modification of the traditional FPM algorithm with complex pupil recovery [1, 5, 10]. A pseudo-MATLAB code is provided here

$$H(k) = \mathrm{ScaledFFT}(h(j), s) \quad (2)$$

```
Define kx, ky vectors for LEDs,
CCD pixel size spsize,
high-resolution pixel size psize,
low-resolution matrix size m1 x m1,
high-resolution matrix size m x m,
read images, do background removal,
Define scaled FFT fraction s1=0.25,
dk=s1*2*pi/(psize*m);
kmax=s1*pi/spsize;% max rad/m freq,
kaxis=-kmax:dk:kmax-dk; % rad/m
CTF=(kaxis.^2+kaxis.^2)<=cutoffFrequency^2;
scaled FFT factor s=s1/m;% s=1/m for usual DFT
```


1350911x, 2021, 3, Downloaded from https://ietresearch.onlinelibrary.wiley.com/doi/10.1049/ell2.12081 by Readcube (Labtiva Inc.), Wiley Online Library on [01/12/2022]. See the Terms and Conditions (https://onlinelibrary.wiley.com/terms-and-conditions) on Wiley Online Library for rules of use; OA articles are governed by the applicable Creative Commons License

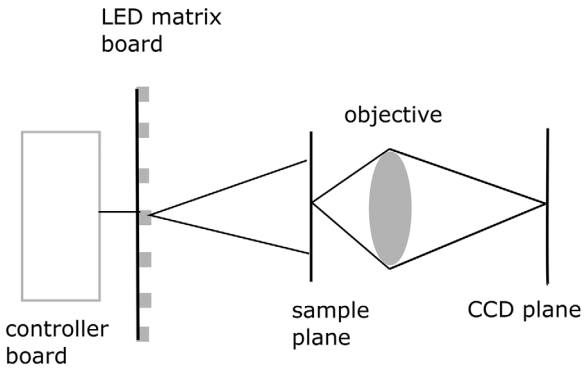

Fig. 1 *Schematic diagram of the experimental setup*

```
objectRec=upscaled bright-field image size mxm;
objectRecFT=ScaledFFT(objectRecover,s);
Pupil_Rec = CTF; % Unknown complex pupil
for loop=1:1:max_itertions
for LED_no=1:1:end
% center of the shifted pupil
kxc=round(n/2+1-kx(LED_no)/dk);
kyc=round(m/2+1-ky(LED_no)/dk);
% lower and upper limits of shifted pupil
kxl=round(kxc-n1/2);
kxh=round(kxc+n1/2)-1;
kyl=round(kyc-m1/2);
kyh=round(kyc+m1/2)-1;
O_j = objectRecFT(kyl:kyh,kxl:kxh);
lowResFT1 = O_j.*pupil_Rec;
% forward image
imLowRes=(s^2)*ScaledFFT(lowResFT1, -s*m/m1));
imLowRes=(m/m1)^2*sqrt(Image(LED_no))
.*exp(j*angle(imLowRes));
lowResFT2=ScaledFFT(imLowRes,s*m/m1);
% update the object sub-spectrum
objectRecFT(kyl:kyh,kxl:kxh)=O_j+abs(pupil.*CTF).*
conj(Pupil_Rec)./max(max(abs(Pupil_Rec)))
./(abs(Pupil_Rec).^2+1.0).*(lowResFT2-lowResFT1);
% update the complex pupil
Pupil_Rec=Pupil_Rec+abs(O_j).*conj(O_j.*CTF)./
max(max(abs(O_j)))
./(abs(O_j).^2+1000.0).*(lowResFT2-lowResFT1);
end
end
objectRechi=(s)^2*ScaledFFT(objectRecFT,-s);
```

Recovery from experimental images: A schematic of the setup is shown in Figure 1. The following hardware was used for taking experimental images: Basler camera (Model acA5472-17um, pixel size 2.4 μm × 2.4 μm, 12-bit resolution), 15 × 15 LED board with LED spacing 4 mm, wavelength 0.52 μm, LED to sample plane distance =113 mm for USAF target, =103 mm for bone sample, optics NA = 0.08, magnification 4x. The central 256 × 256 pixels of the captured low-resolution images were used to reconstruct the high-resolution image with an up-scaling ratio of 4 giving high-resolution matrix size 1024 × 1024, $NA_{synthetic}$ = 0.47 for the corner LEDs was recovered and 10 iterations of the recovery loop were run.

The FPM recovery results are given in Figures 2 and 3 for the USAF resolution target (which is an amplitude target) and for the cartilage bone sample (which is a complex target), respectively. In Figure 2, group 9 element 3 is clearly resolved by both algorithms. It can be seen in these figures that the quality of recovery of the high-resolution object (both amplitude and phase) is similar in both algorithms with some artefacts due to the presence of noise in the captured images, as no noise removal was performed on the captured images. The main advantage of the scaled FFT scheme is that the recovered spectrum of the object covers a bigger area of the 1024× 1024 matrix, thus showing finer details of the spectrum. In addition, the recovered pupil amplitude and phase also

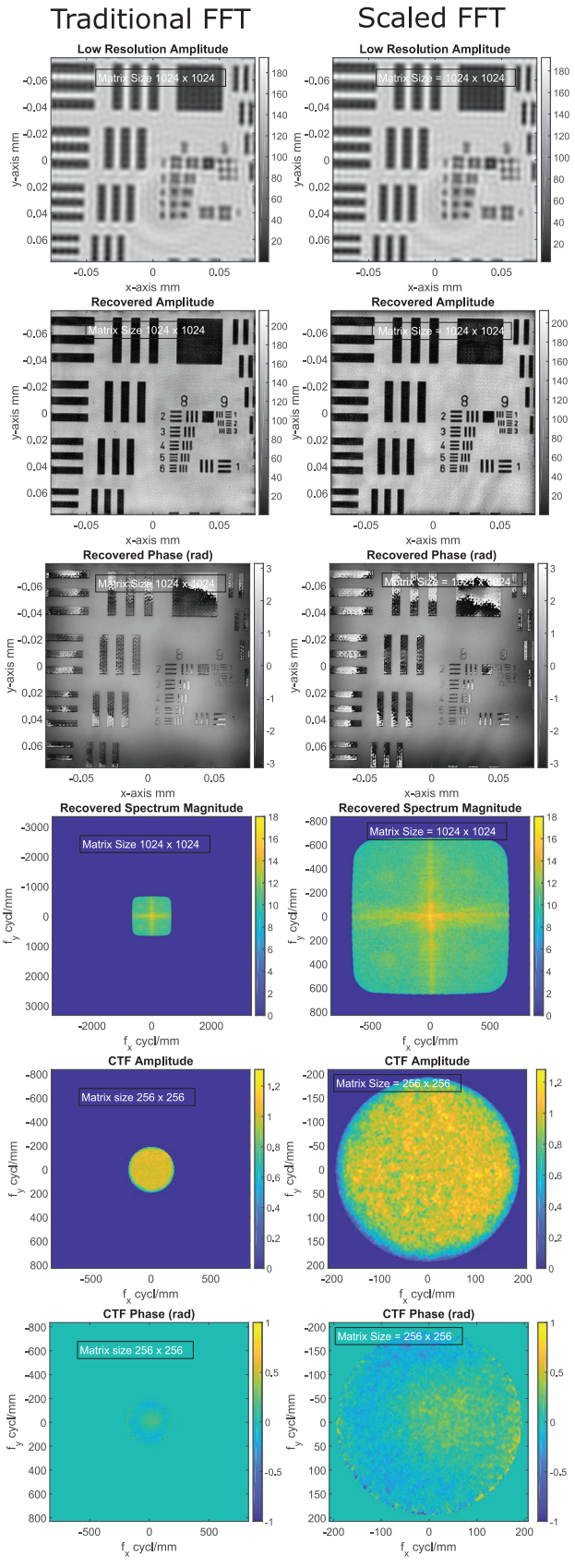

Fig. 2 *Traditional FFT versus scaled FFT (s_1 = 0.25) FPM recovery, USAF amplitude target*

show finer details as compared to the traditional FFT algorithm while having the same matrix size. Note that the maximum resolvable spatial frequency is still the same for both algorithms since that is dictated by the synthetic NA, which remains the same for both cases.

1350911x, 2021, 3, Downloaded from https://ietresearch.onlinelibrary.wiley.com/doi/10.1049/el2.12081 by Readcube (Labtiva Inc.), Wiley Online Library on [01/12/2022]. See the Terms and Conditions (https://onlinelibrary.wiley.com/terms-and-conditions) on Wiley Online Library for rules of use; OA articles are governed by the applicable Creative Commons License

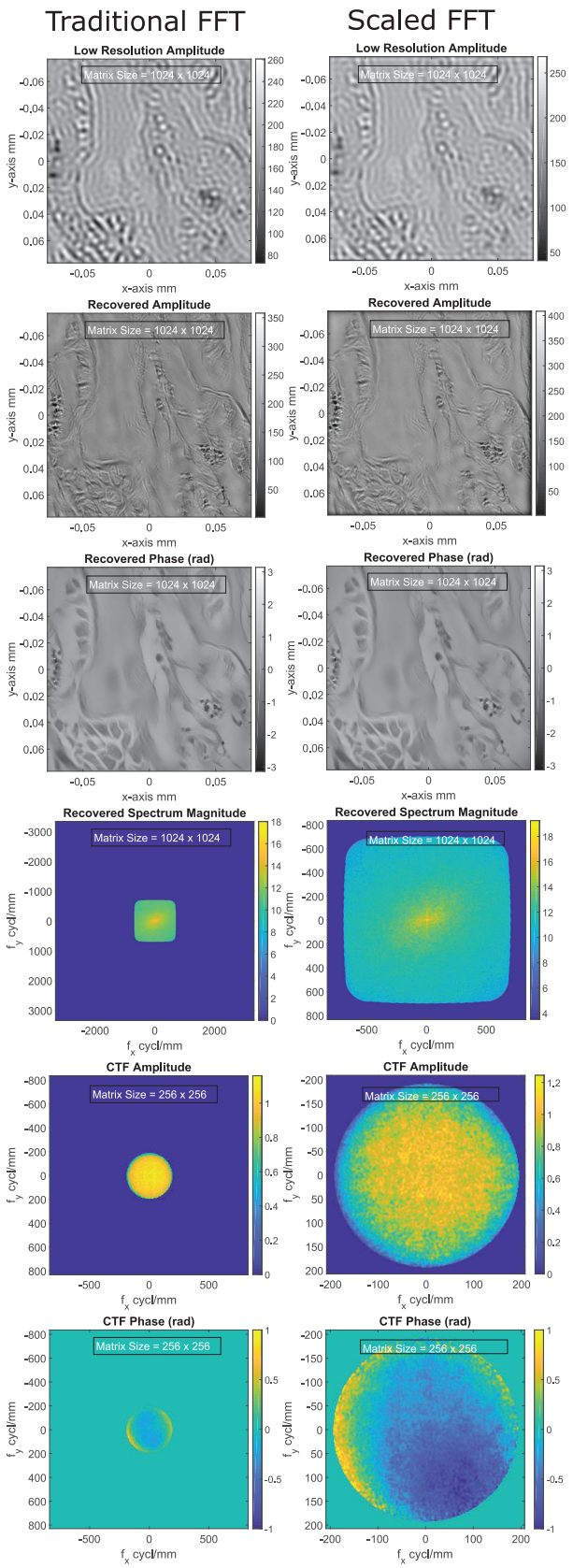

Fig. 3 *Traditional FFT versus scaled FFT ($s_1 = 0.25$) FPM recovery, cartilage/bone sample*

Conclusion: We have derived an FPM recovery scheme based on the scaled FFT. The advantage of the scaled FFT is that the recovered spectrum and the complex pupil function can be zoomed-in to see finer details while keeping the same matrix size as in the traditional FFT-based FPM schemes. Thus, a bigger portion of the chosen matrices is utilised during the FPM recovery process. The results of recovery of experimental images of different samples show that the new algorithm produces good recovery for both amplitude and phase of the object as well as the pupil aberrations. Future work will focus on exploring convergence properties of the FPM algorithm with the scaled FFT.

Acknowledgments: This work was supported by the Research Council of Norway through its CoE funding scheme (262644) and NANO2021 (272248).

© 2021 The Authors. *Electronics Letters* published by John Wiley & Sons Ltd on behalf of The Institution of Engineering and Technology

This is an open access article under the terms of the Creative Commons Attribution License, which permits use, distribution and reproduction in any medium, provided the original work is properly cited.
Received: *19 November 2020* Accepted: *29 December 2020*
doi: 10.1049/ell2.12081

References

1 Zheng, G.: *Fourier Ptychographic Imaging: A MATLAB Tutorial*. Morgan & Claypool, San Rafael, CA (2016)
2 Zheng, G.: Breakthroughs in Photonics 2013: Fourier ptychographic imaging. *IEEE Photonics J.* **6**(2), 0701207 (2014)
3 Guo, K., Dong, S., Zheng, G.: Fourier ptychography for brightfield, phase, darkfield, reflective, multi-slice, and fluorescence imaging. *IEEE J. Sel. Top. Quantum Electron.* **22**(4), 6802712 (2016)
4 Konda, P., et al.: Fourier ptychography: Current applications and future promises. *Opt. Express* **28**(7), 9603–9630 (2020)
5 Guizar-Sicairos, M., Fienup, J.: Phase retrieval with transverse translation diversity: a nonlinear optimization approach. *Opt. Express* **16**(10), 7264–7278 (2008)
6 Goodman, J.W.: *Introduction to Fourier Optics*, 4th ed. W. H. Freeman, San Francisco, CA (2017)
7 Ou, X., et al.: High numerical aperture Fourier ptychography: principle, implementation and characterization. *Opt. Express* **23**(3), 3472–3491 (2015)
8 Bian, Z., Dong, S., Zheng, G.: Adaptive system correction for robust Fourier ptychographic imaging. *Opt. Express* **21**(26), 32400–32410 (2013)
9 Ou, X., Zheng, G., Yang, C.: Embedded pupil function recovery for Fourier ptychographic microscopy. *Opt. Express* **22**(5), 4960–4972 (2014)
10 Tian, L., Waller, L.: 3D intensity and phase imaging from light field measurements in an LED array microscope. *Optica* **2**(2), 104–111 (2015)
11 Zhang, Y., Pan, A., Lei, M.: Data preprocessing methods for robust Fourier ptychographic microscopy. *Opt. Eng.* **56**(12), 123107–1231013 (2017)
12 Konda, P.C.: Multi-aperture Fourier ptychographic microscopy: Development of a high-speed gigapixel coherent computational microscope. Ph.D. dissertation, University of Glasgow (2017).
13 Pan, A., et al.: Vignetting effect in Fourier ptychographic microscopy. *Opt. Lasers Eng.* **120**, 40–48 (2019)
14 Muffoletto, R., Tyler, J., Tohline, J.: Shifted fresnel diffraction for computational holography. *Opt. Express* **15**(9), 5631–5640 (2007)
15 Bailey, D., Swarztrauber, P.: The fractional Fourier transform and applications. *SIAM Rev.* **33**(3), 389–404 (1991)
16 Shimobaba, T. et al.: Computational wave optics library for C++: CWO++ library. *Comput. Phys. Commun.* **183**(5), 1124–1138 (2012)

1350911x, 2021, 3, Downloaded from https://ietresearch.onlinelibrary.wiley.com/doi/10.1049/ell2.12081 by Readcube (Labtiva Inc.), Wiley Online Library on [01/12/2022]. See the Terms and Conditions (https://onlinelibrary.wiley.com/terms-and-conditions) on Wiley Online Library for rules of use; OA articles are governed by the applicable Creative Commons License